RSC Sustainability

ROYAL SOCIETY OF CHEMISTRY

PAPER

View Article Online
View Journal | View Issue

Cite this: *RSC Sustainability*, 2025, **3**, 486

Study of adsorption efficiencies of biopolymer-based composites of chitosan with a sulfonic acid functionalized imidazolium ionic liquid for elimination of organic dyes in wastewater†

Subham Paul, Amlan Jyoti Gogoi, Krishna Dev, Prapti Priyam Handique, Debanga Bhusan Bora, Sangeeta Kalita and Ruli Borah *

In the present work, Brønsted acidic ionic liquid 2-methyl-*N*,*N*-disulfoimidazolium chloride [Mdsim]Cl impregnated chitosan composites were prepared by mixing chitosan with [Mdsim]Cl in different ratios. The prepared composites were characterized by FT-IR, PXRD, SEM and TGA techniques. The adsorption behaviour of the prepared composites was efficiently investigated for the removal of methylene blue (MB), as a cationic model dye compound from aqueous solution. Various concentrations of aqueous MB dye solutions were used to study the adsorption nature of composites through UV studies. The adsorption kinetics of MB was well described using a pseudo-second-order model and intra-particle diffusion model. The adsorption also followed the Langmuir adsorption isotherm and the maximum adsorption capacity was 2.3 mg g^{-1} among the prepared composites. The adsorption capacity of the composite was also compared with three other dyes, namely methyl orange, crystal violet and methyl green.

Received 21st August 2024
Accepted 27th November 2024

DOI: 10.1039/d4su00501e

rsc.li/rscsus

Sustainability spotlight

The discharge of wastewater containing various organic pollutants into the environment without treatment from different industries like textile, printing, leather tanning, cosmetics, food processing, *etc.* poses many health hazards to human, animal and aquatic lives. Dyes are one of the toxic pollutants and cause direct threat to both aquatic lives and lives on land when come into contact. Here, a sustainable composite material is developed through combination of cheap and available biopolymer chitosan with functionalized ionic liquids as recyclable adsorbents for organic dyes. Thus, our work can help to fulfil the Sustainable Development Goals (SDGs) 6, 14 and 15 of the United Nations.

1. Introduction

Dyes are usually discharged into water bodies as waste materials used in industries such as textile, printing, leather tanning, cosmetics, food processing, *etc.*[1,2] This can lead to significant environmental problems when they interact with aquatic life and cause serious health hazards in human beings like hypertension, blurred vision, abdominal pain, dizziness, abnormal urine, asthma, nausea, itching, staining of skin, carcinogenic effects, *etc.*[3] So, removal of these dyes from aquatic regions is of great demand and various chemical, physical, and biological methods have been developed for this purpose. These include chemical oxidation,[4] electrochemical oxidation,[5] photo-degradation,[6] reduction,[7] biological treatment,[8] adsorption,[9] coagulation–flocculation[10] and membrane separation.[11] Most of these methods suffer from drawbacks like generation of toxic sludge and high operation and maintenance costs. Among these methods, the adsorption techniques have several advantages like cost effectiveness, simple design and operation, no production of toxic by-products, possibility for regeneration of adsorbents, removal of different pollutants under varied conditions including pH, temperature, initial dye concentration, contact time, adsorbent dose, *etc.*[3] For the removal of wastewater dye pollutants, various adsorbents like carbon-based materials, polymer-based materials, bio-adsorbents, metal oxides, clays, *etc.* have been employed efficiently, but some of them have drawbacks because of their difficulty in regeneration and high cost.[3,12,13]

Natural biopolymers are considered as potential adsorbents for treatment of wastewater due to their abundance and cost-effectiveness, specific structures with functional groups to design new adsorbents, chemical stability, unique physico-chemical properties, ecofriendliness, biodegradability, and ability to bind different pollutants through physical and chemical interactions.[14–16] Chitin and chitosan are such natural

Department of Chemical Sciences, Tezpur University, Napaam, 784028, Tezpur, Assam, India. E-mail: ruli@tezu.ernet.in

† Electronic supplementary information (ESI) available. See DOI: https://doi.org/10.1039/d4su00501e

polysaccharides with definite physical, chemical, and biological properties. Usually, the chitosan is derived as a partially deacetylated derivative of biopolymer chitin, *i.e.* poly(β-(1–4)-*N*-acetyl-D-glucosamine), containing repeating units of *N*-acetyl-D-glucosamine and D-glucosamine.[17,18] The existence of –OH, –NH_2 and –$NHCOCH_3$ functionalities on the surface of chitosan provides adsorption capabilities of organic pollutants through H-bonding, intermolecular interaction, and electrostatic attraction. Despite this, it suffers from disadvantages including low adsorption capacity, poor mechanical strength, and low recyclability because of poor physicochemical properties such as morphological nature, surface area, thermal stability, functional groups, *etc.*[19]

To overcome the above limitations of pure chitosan as an adsorbent, different chemical or physical modifications have been reported by incorporating reinforcement materials like carbon-based materials, zeolites, metal oxides and other biopolymers in the chitosan matrix to develop chitosan composites.[20,21] In this context, functionalized ionic liquids can be used as reinforcement materials to increase the surface functionalities of chitosan for improvement of adsorption efficiencies along with other physicochemical properties such as mechanical strength, thermal stability, pH sensitivity, surface area, *etc.* The review on ionic liquid modified composites of different adsorbents also mentioned improved adsorption efficiencies for water pollutants.[22] As functional materials, ionic liquids (ILs) represent a class of prospective materials with tunable physicochemical properties, which exist in the liquid state below 100 °C. They are non-flammable viscous organic salts prepared by a proper combination of organic cations with organic or inorganic anions depending on the desired physicochemical characteristic. Their variable physicochemical behavior includes viscosity, polarity, hydrophilic/hydrophobic nature, conductivity, density, surface tension, thermal and electrochemical stability, moisture sensitivity, ability to dissolve organic/inorganic or other materials, *etc.*[23–25] The properties of ionic liquids can also be varied by incorporation of functional groups like –SO_3H, –COOH, –OH, *etc.* into their constituent ions, making them suitable for use as greener reaction medium, catalysts, electrolytes, and surfactants, in separation and purification technology such as liquid–liquid extraction, liquid–solid phase extraction, microextraction, *etc.* It has been observed that chitosan provides a biocompatible matrix for immobilization of functionalized ionic liquids by physical and chemical modifications with transfer of specific properties of ionic liquids to the chitosan–ionic liquid composites leading to enhancement of overall stability, making them suitable for a wide range of applications. These include the design of new catalysts, pollutant scavengers, chemical sensors, drug delivery systems, adsorption of heavy metal ions, antimicrobial activity, biomedical fields, *etc.*[26]

From these prospectives, it was aimed to develop (Scheme 1) various composites of chitosan impregnated with different amounts of Brønsted acidic ionic liquid 2-methyl-*N*,*N*-disulfoimidazolium chloride [Mdsim]Cl[27] to investigate their adsorption efficiencies for the removal of the cationic model dye

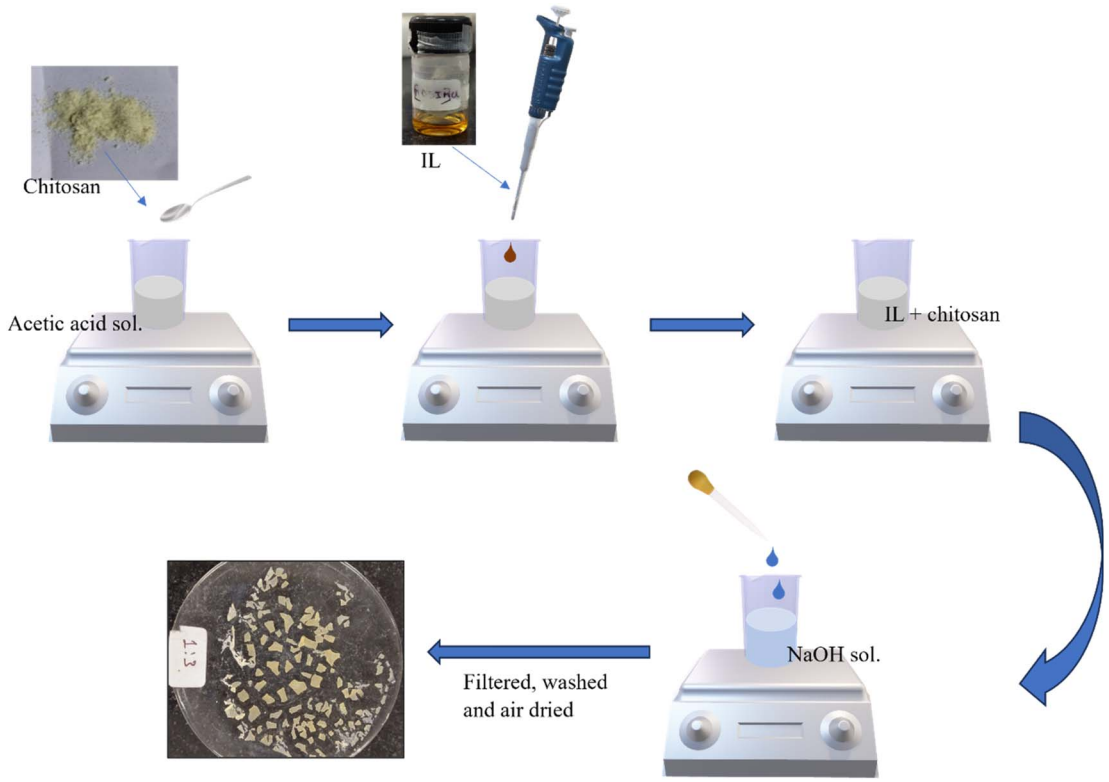

Scheme 1 Representative procedure for preparation of chitosan–IL composites.

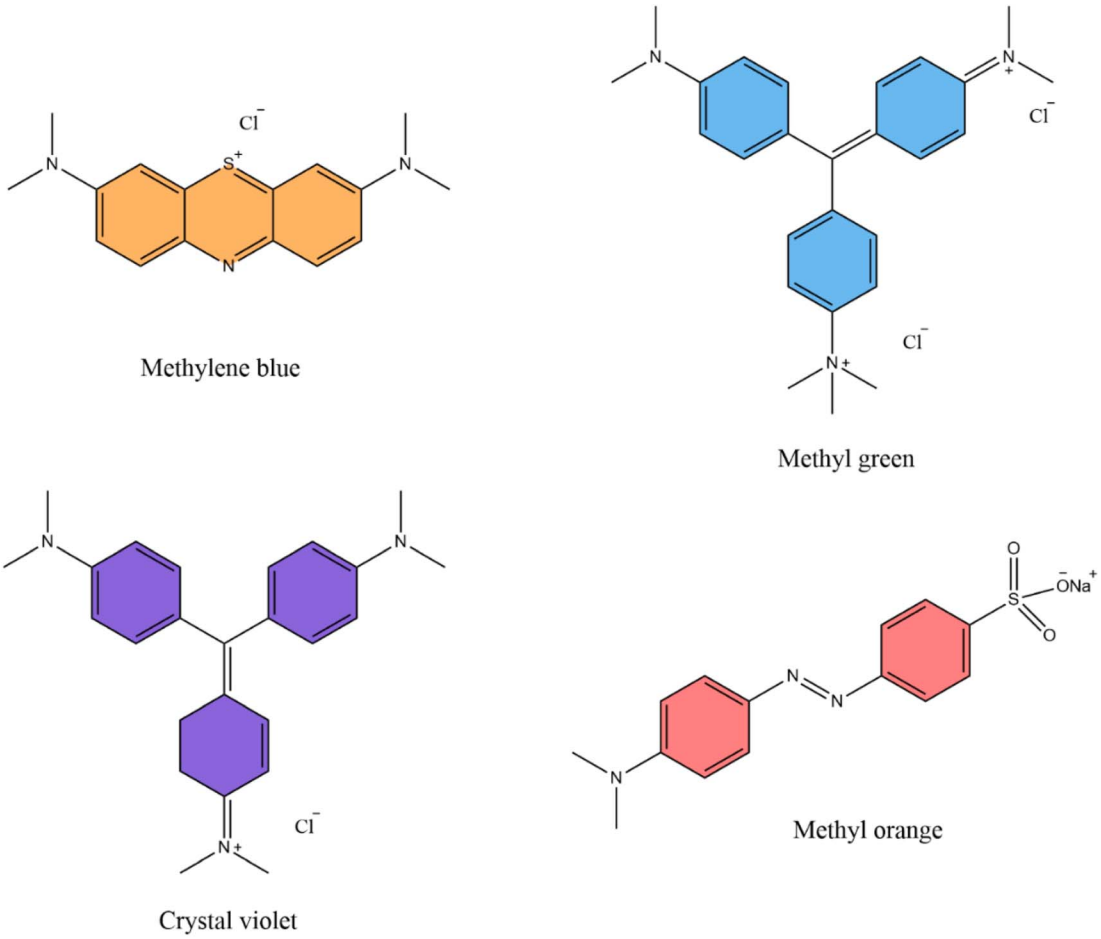

Fig. 1 Structure of organic dye molecules.

methylene blue (MB) (Fig. 1) in aqueous solution with various adsorption parameters as well as adsorption isotherm, kinetic, and thermodynamic analysis.

2. Materials and methods

2.1. Materials

All required analytical grade chemicals were procured from chemical suppliers Merck, Rankem Chemicals, Sisco Research Pvt. Ltd (India), SD Fine Chem Ltd and Loba Chemie in pure states to prepare the ionic liquid [Mdsim]Cl and the chitosan–ionic liquid composite material. These included chitosan (molecular weight: ~193 400 g mol^{-1}), 2-methyl imidazole (>99%), chlorosulfonic acid (97%), NaOH, and glacial acetic acid. All the stock solutions of MB were prepared in freshly prepared deionized double distilled water to study the adsorption performances of the composite material.

2.2. Methods

A PerkinElmer MIR-FIR FT-IR spectrophotometer was employed for recoding the FT-IR spectra of the chitosan–IL composites within 4000–400 cm^{-1} using KBr pellets. The morphological images of the composites were determined using a scanning electron microscope (SEM), model: JEOL JSM-6390LVSEM. Thermogravimetric analysis of the composites was conducted using a Shimadzu TGA-50 analyzer. A Shimadzu UV-1800 UV spectrophotometer was employed to measure the MB concentrations during adsorption studies.

2.3. Preparation of 2-methyl-*N*,*N*-disulfoimidazolium chloride [Mdsim]Cl

The preparation of the 2-methyl-*N*,*N*-disulfoimidazolium chloride [Mdsim]Cl ionic liquid was done as per a standard method.[27] The procedure involved dropwise addition of 20 mmol of chlorosulfonic acid at 0 °C to a solution of 10 mmol of imidazole in 15 mL of dry dichloromethane (DCM) in a 100 mL round bottom flask with continuous stirring for 30 min to form a DCM immiscible viscous layer of the ionic liquid. The viscous layer of IL was washed three times with dichloromethane (3 × 5 mL) after removal of the initial solution of DCM by decantation. The crude ionic liquid was dried in a vacuum oven at 60 °C for 3 h to obtain the pure ionic liquid.

2.4. Preparation of chitosan–[Mdsim]Cl composites

For the synthesis of chitosan–[Mdsim]Cl composites, 0.50 g of chitosan was dissolved in 50 mL solution of acetic acid (2% v/v)

taken in a 100 mL beaker, followed by addition of 0.50 g of [Mdsim]Cl to the solution with continuous stirring for 2 h. The obtained solution was then added dropwise to an aqueous 1 M NaOH (100 mL) solution and stirred for 2 h to obtain a solid precipitate. It was then filtered and washed with distilled water 2–3 times and dried in air for 24 h. By using this procedure (Scheme 1), the chitosan composites of the ionic liquid were made in three ratios (1 : 1, 1 : 2 and 1 : 3) by taking 0.50 g, 1 g and 1.5 g of [Mdsim]Cl, respectively, against 0.50 g of the chitosan.

2.5. Adsorption experiments

To evaluate the adsorption properties of the composites, adsorption experiments were performed in batch mode (Scheme 2) by adding specific amounts of the chitosan–[Mdsim]Cl composites (5–40 mg) to each 10 mL of the MB stock solution (2.5, 5, 10 and 20 mg L^{-1}) and stirred at room temperature for a specific period. In the next step, the sorbent was separated, and the concentration of MB solution was determined using a UV-Vis spectrophotometer at the maximum wavelength $\lambda_{max} =$ 664 nm by plotting the absorbance value of MB *versus* concentration with a linear relationship through the Beer–Lambert law. The removal percentage R (%) and adsorption capacity at equilibrium q_e and t time q_t (mg g^{-1}) of the sorbent were calculated from eqn (1)–(3), respectively.[28]

$$R(\%) = \frac{C_0 - C_t}{C_0} \times 100 \quad (1)$$

$$q_e = \frac{C_0 - C_e}{m} \times V \quad (2)$$

$$q_t = \frac{C_0 - C_t}{m} \times V \quad (3)$$

Here, C_0, C_e and C_t are the concentrations of the MB stock solution at the initial, equilibrium and time t, respectively. V is the volume of MB solutions, and m is the amount of absorbent in grams.

2.6. Study of adsorption kinetics

To investigate the adsorption kinetics of MB adsorption on the chitosan–IL composites, three kinetic models eqn (4)–(6) were employed to fit the experimental data (Table S1†) for pseudo-first-order, pseudo-second order and Weber and Morris

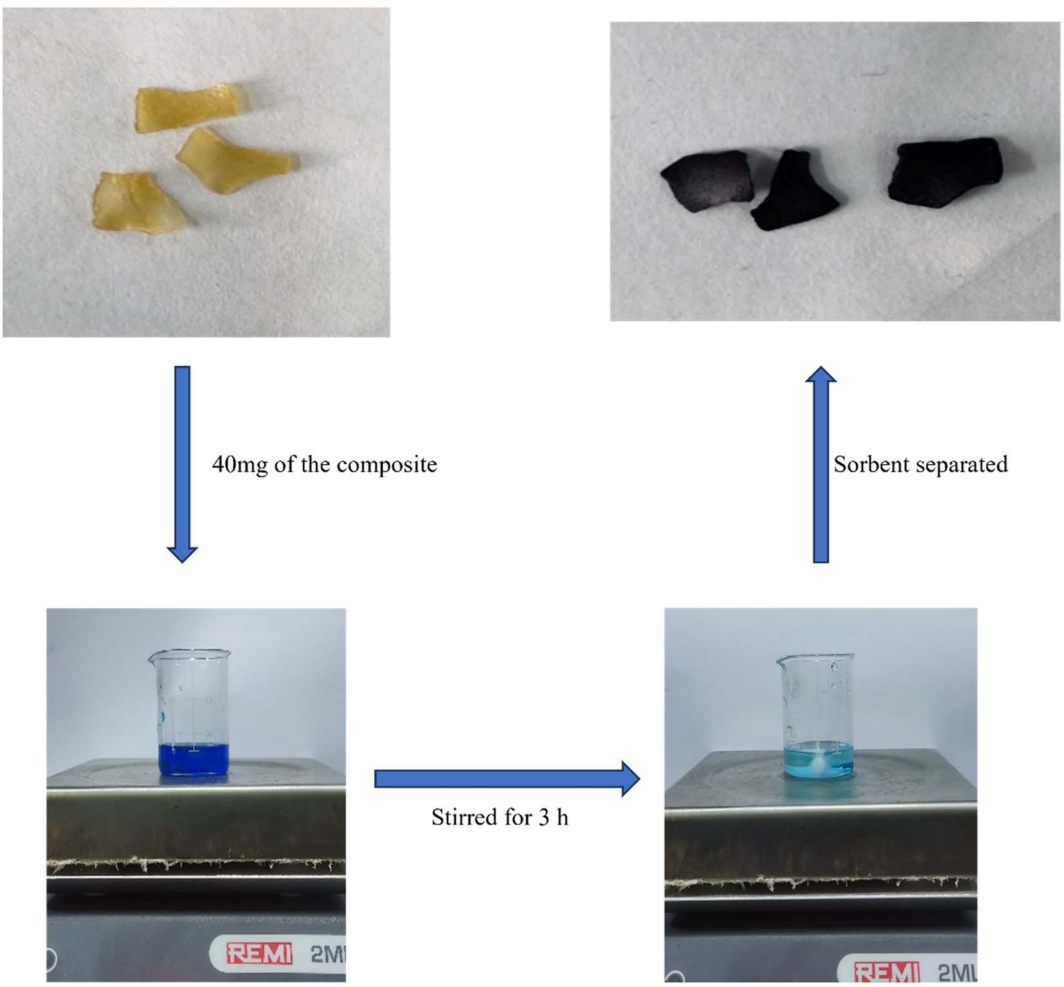

Scheme 2 Representative method for adsorption of MB dye solution using chitosan–IL composites.

Table 1 Calculated adsorption kinetic parameters for MB adsorption

		Pseudo-first order (linear)			Pseudo-second order (linear)			Intra-particle diffusion model		
C_0 (mg L^{-1})	$q_{e,exp}$ (mg g^{-1})	$q_{e,cal}$ (mg g^{-1})	k_1	R^2	$q_{e,cal}$ (mg g^{-1})	k_2	R^2	K_{i1}	K_{i2}	K_{i3}
10	1.95	2.43	0.0078	0.042	1.705	5.573	0.977	3.230	0.197	−0.40

Table 2 Calculated isotherm model parameters

		Langmuir (linear)				Freundlich (linear)		
T (°C)	$q_{m,exp}$ (mg g^{-1})	$q_{m,cal}$ (mg g^{-1})	K_L	R^2	R_L	K_F	n	R^2
25	2.35	2.67	0.75	0.993	0.062–0.347	0.99	2.22	0.838
35	1.45	1.80	0.32	0.981	0.136–0.559	0.44	1.93	0.880
45	2.35	4.17	0.12	0.928	0.294–0.769	0.48	1.46	0.988

models, respectively. The calculated parameters of the three models are included in Table 1.

$$\ln(q_e - q_t) = \ln q_e - k_1 t \quad (4)$$

where k_1 (min^{-1}) is the rate constant of the pseudo-first order model and this value was determined from the slope of the linear plot of $\ln(q_e - q_t)$ *versus* time (t).[29,30]

$$\frac{t}{q_t} = \frac{1}{k_2 {q_e}^2} + \frac{t}{q_e} \quad (5)$$

Here k_2 (g mg^{-1} min^{-1}) is the rate constant of the pseudo-second order model.[31] Using eqn (5), the rate constant value k_2 and the amount of MB adsorbed at equilibrium (q_e) were calculated from the intercept ($1/k_2 {q_e}^2$) of the straight line by plotting t/q_t *versus* time (t) with a slope of $1/q_e$.

The intraparticle diffusion model of Weber–Morris[32] eqn (6) was employed to observe the diffusion mechanism of MB adsorbed at different time intervals with the intraparticle diffusion constant K_i (mg g^{-1} $min^{1/2}$) involving various steps of adsorption including bulk diffusion, film diffusion, particle diffusion and chemical reactions.[33]

$$q_t = K_i t^{1/2} + C \quad (6)$$

The slope of the straight line of q_t *versus* $t^{1/2}$ provided the intraparticle diffusion constant K_i.

2.7. Study of adsorption isotherms

Two well-known isotherms, Langmuir and Freundlich models, were employed to evaluate the experimental data of adsorption of MB dyes (Table S2†) with varied concentrations (2.5, 5, 10 and 20 mg L^{-1}) and temperatures (298, 308, and 318 K) on the composite using eqn (7) and (8), respectively.[28] The calculated parameters of the two models are included in Table 2.

$$q_e = \frac{q_m K_L C_e}{1 + K_L C_e} \quad (7)$$

$$e = K_f {C_e}^{1/n} \quad (8)$$

where q_m is the maximum adsorbent capacity (mg g^{-1}), K_L (L g^{-1}) is the Langmuir constant, K_f is the Freundlich constant and n is the favorability of the adsorption process.

The linear equations of Langmuir and Freundlich models can be displayed by eqn (9) and (10) as given below.

$$\frac{C_e}{q_e} = \frac{1}{q_m K_L} + \frac{C_e}{q_m} \quad (9)$$

Here, the slope of the linear plot C_e/q_e *versus* C_e/q_m was used to determine the value of maximum adsorbent capacity (q_m) and the Langmuir constant (K_L) from the intercept ($1/q_m K_L$) value.

$$\ln q_e = \ln K_f + 1/n \ln C_e \quad (10)$$

From this equation, the intercept of the linear plot of $\ln q_e$ *versus* $\ln C_e$ was used to calculate the value of the Freundlich constant (K_f) and the favorability of the adsorption process (n) from the slope ($1/n$).

3. Results and discussion

To perform the adsorption studies of the chitosan-based composite of [Mdsim]Cl for aqueous organic dye solutions, initially three different ratios (1 : 1, 1 : 2 and 1 : 3) of chitosan and ionic liquids were employed for the preparation of the three types of composites (Scheme 1) using 0.50 g, 1 g and 1.5 g of the [Mdsim]Cl ionic liquid against 0.50 g of the chitosan, respectively.

3.1. Characterization of chitosan–IL composites

The structural characteristics and thermodynamic stability of the composites were determined using FT-IR, SEM, powder XRD, and thermogravimetric analyses.

Initially, the comparative FT-IR spectra of chitosan, [Mdsim]Cl and the 1 : 3 chitosan–[Mdsim]Cl composite are displayed in Fig. 2. The various peaks of chitosan can be observed at 3438 cm^{-1} (overlapped stretching vibrations of O–H and N–H bonds), 2924 cm^{-1} (C–H stretching), 1412 cm^{-1} (angular deformation of the $-CH_3$ group), 1561 cm^{-1} (merged N–H

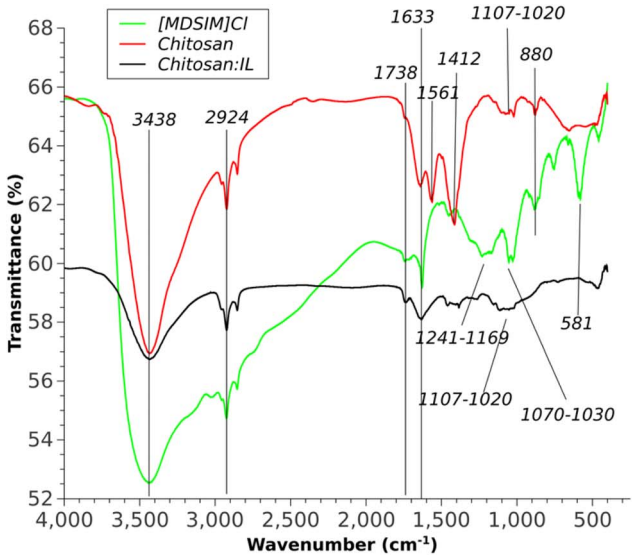

Bonds	Peaks
O-H and N-H stretching	3438
C-H stretching	2924
C=C and C=N stretching	1738
C=O stretching vibration	1633
N-H bending and C-N stretching	1561
Angular deformation-CH_3	1412
S-O asymmetric stretching	1241-1169
stretching of C-O-C bridge	1107-1020
S-O symmetric stretching	1070-1030
N-S stretching	880
S-O bending	581

Fig. 2 FTIR spectra of chitosan, chitosan–IL and [Mdsim]Cl.

bending vibration of amide II and C–N stretching vibrations), 1633 cm^{-1} (C=O stretching vibration of amide band-I) and 1107 cm^{-1} (asymmetric stretching of C–O–C bridge).[34] The spectrum of [Mdsim]Cl showed the existence of $-SO_3H$ groups attached to the organic cation by assigning absorption peaks at 1241–1169 cm^{-1}, 1070–1030 cm^{-1} and 581 cm^{-1} to S–O asymmetric stretching, symmetric stretching, and bending vibrations. The N–S stretch was observed at 880 cm^{-1}. The C=C and C=N stretching vibrations of the imidazolium ring can be observed in similar regions around 1738–1633 cm^{-1}. The IL also exhibited C–H stretching in the same region of chitosan. The broad O–H stretching peak indicated extensive intermolecular H-bonding among the IL molecules.[35] In contrast, the chitosan–[Mdsim]Cl (1 : 3) composite displayed a distinct reduction of peak intensities for the O–H stretching, N–H bending, S–O stretching, and bending vibrations as well as the C=O stretching of the amide I band. A wide peak centered at 1100 cm^{-1} also evidenced strong intake of the Brønsted acidic IL in the chitosan structure. These changes of characteristic peak positions and intensities can be attributed to the efficient interactions of the amide, $-NH_2$ and –OH groups of chitosan with the two $-SO_3H$ groups of 2-methyl 1,3-disulfoimidazolium chloride in the chitosan–IL composite. Interestingly, the composite retains the same peak position and intensity of the C–H stretching vibrations of the methyl substituent.

Fig. 3 shows comparative FT-IR spectra of the three composites and showed the existence of NH_3^+ cations through a N–H stretching at 2354 cm^{-1} for the 1 : 1 and 1 : 2 loaded composites due to protonation of the free $-NH_2$ group of the chitosan,[28,36] whereas this peak was absent in the 1 : 3 loaded

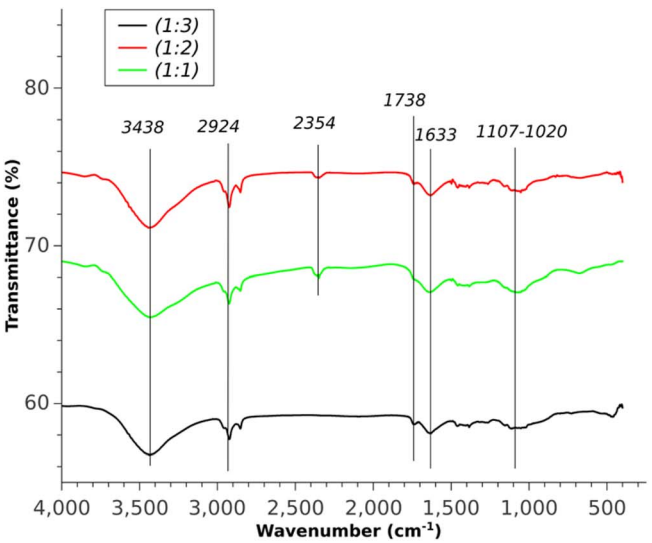

Bonds	Peaks
O-H and N-H stretching	3438
C-H stretching	2924
NH_3^+	2354
C=C and C=N stretching	1738
C=O stretching vibration	1633
stretching of C-O-C bridge	1107-1020
S-O symmetric stretching	1070-1030

Fig. 3 Comparative FT-IR spectra of chitosan–IL composites.

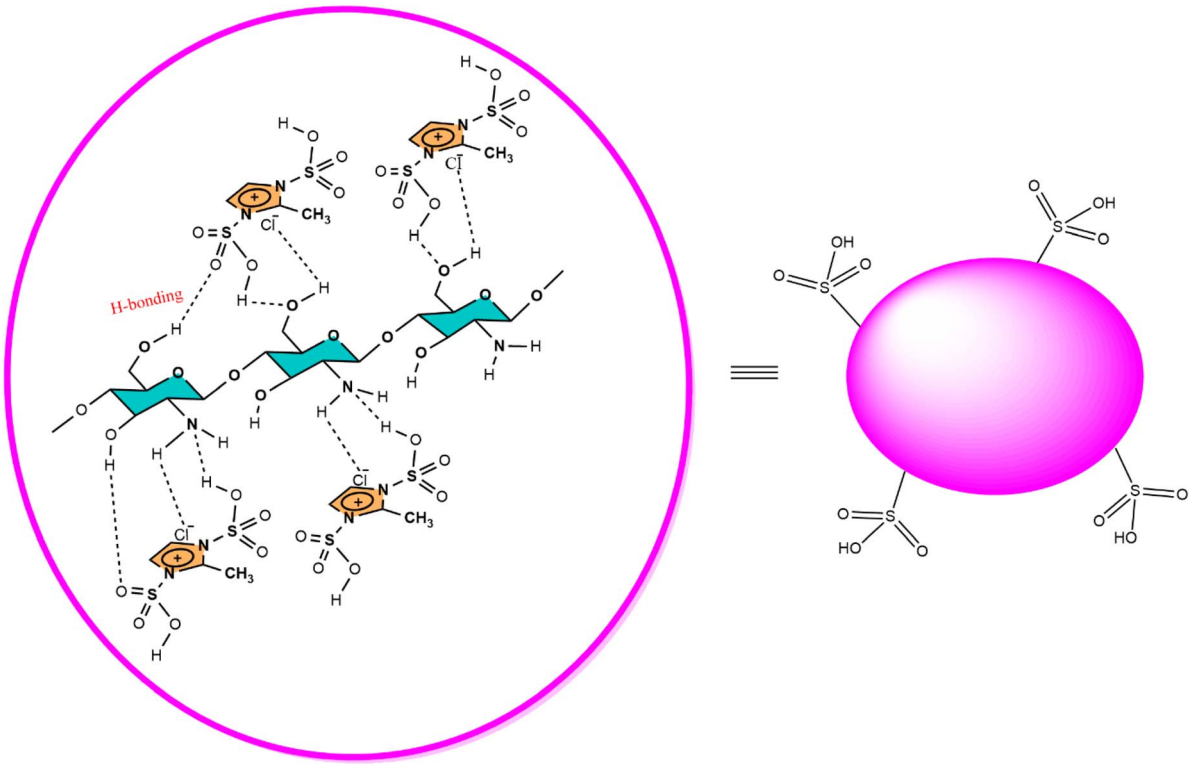

Fig. 4 Proposed structure of the chitosan composite with the [Mdsim]Cl ionic liquid.

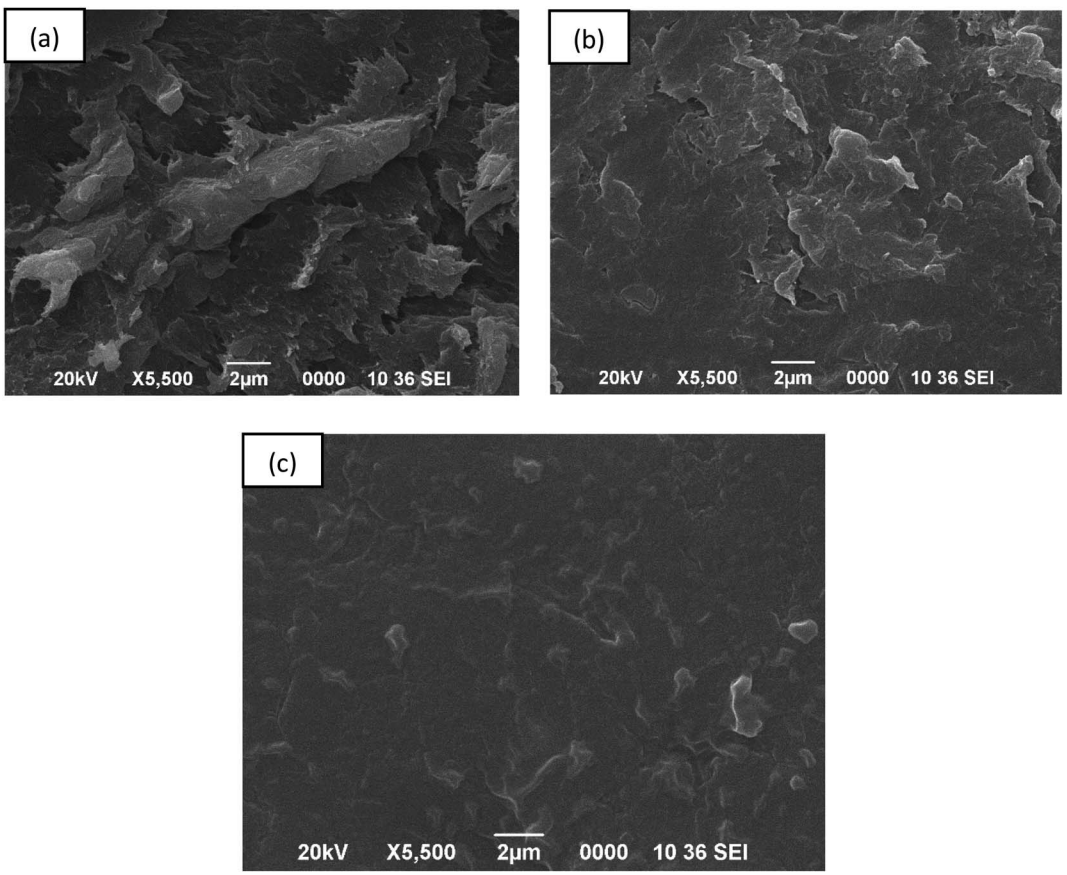

Fig. 5 SEM image of (a) chitosan, (b) the chitosan–IL composite (1 : 3) and (c) the dye adsorbed chitosan–IL (1 : 3) composite.

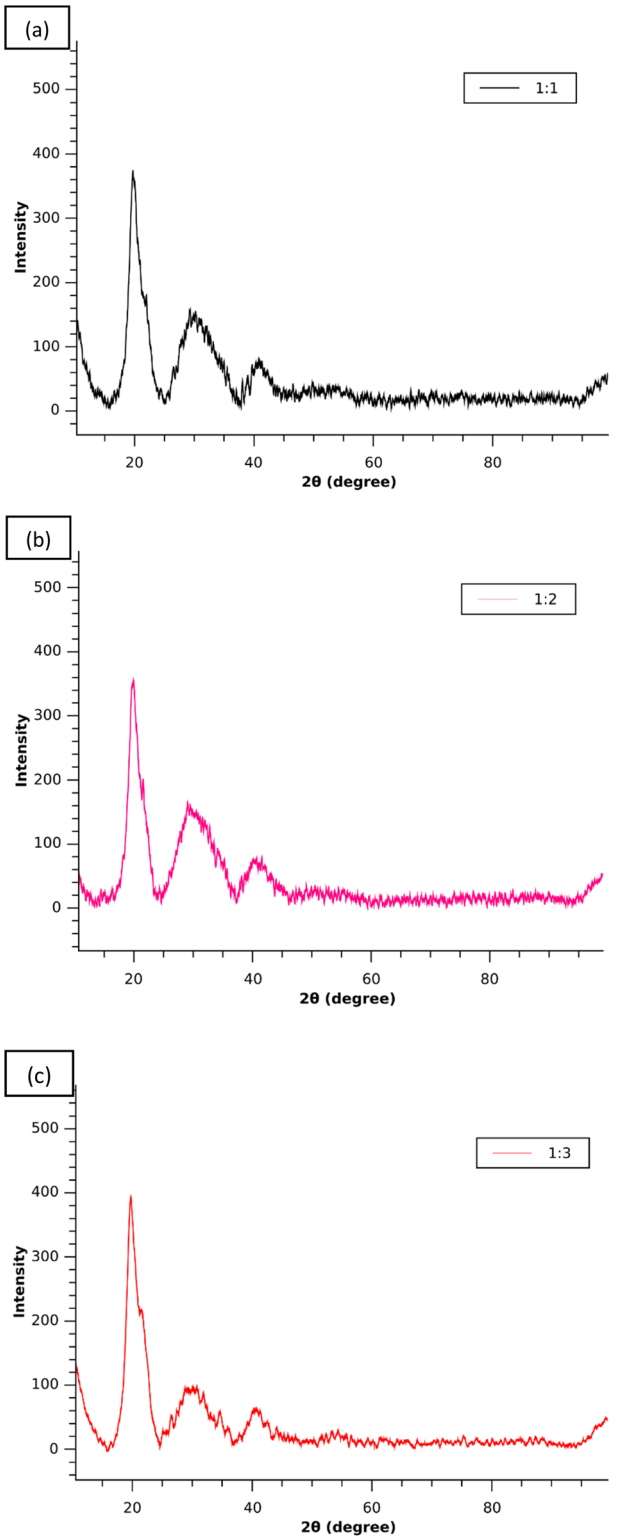

Fig. 6 Comparative PXRD pattern of chitosan–[Mdsim]Cl composites of different ratios (a) 1 : 1, (b) 1 : 2 and (c) 1 : 3.

composite. This observation indicated that with increasing concentration of sulfonic acid functionalized ionic liquid, the free $-NH_2$ groups of chitosan are involved in strong intermolecular H-bonding interactions with one of the $-SO_3H$ groups of

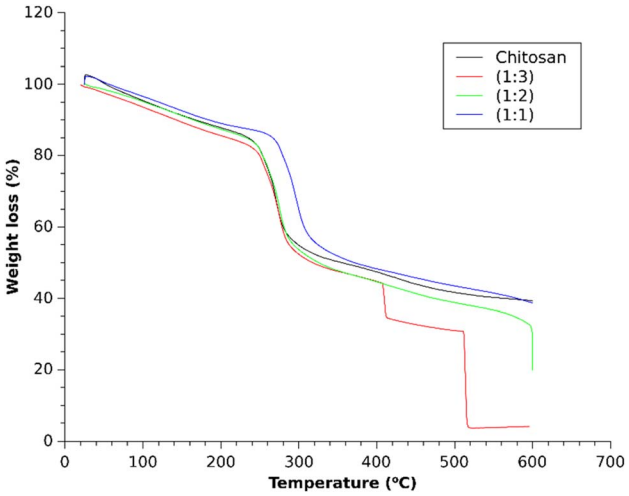

Fig. 7 TGA profile of different chitosan–IL composites.

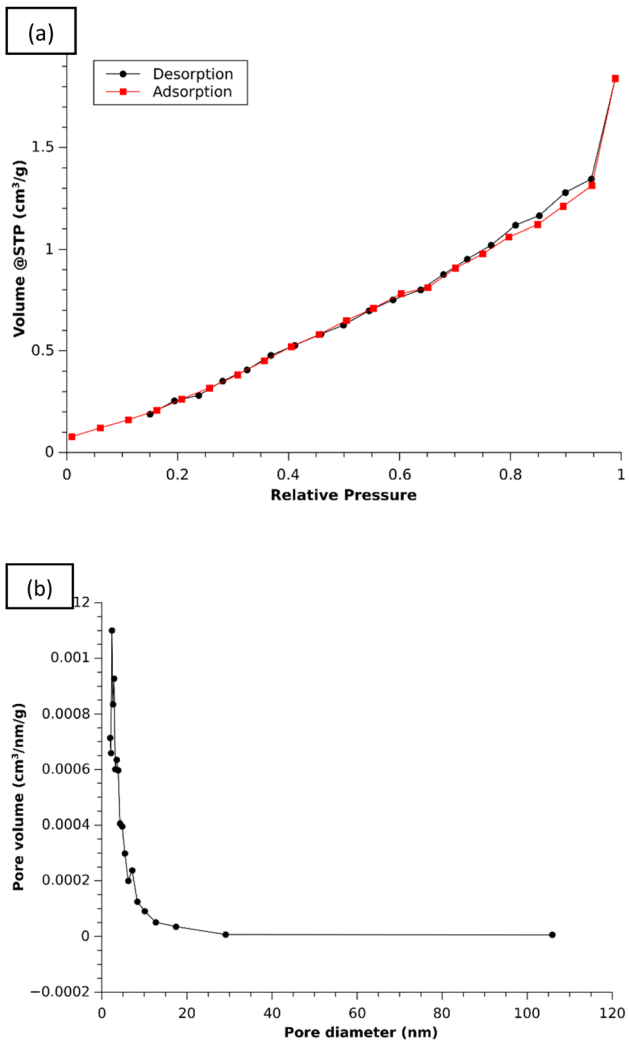

Fig. 8 (a) N_2 adsorption–desorption isotherm and (b) BJH plot.

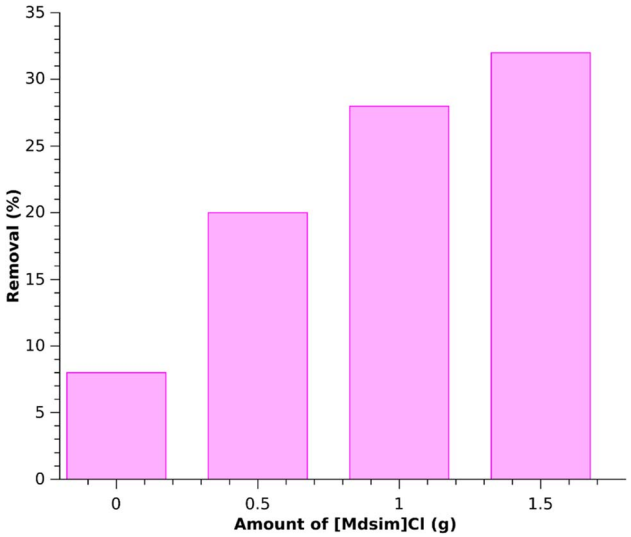

Fig. 9 Effect of [Mdsim]Cl amount on the adsorption behaviour of the composites.

the ionic liquid and thereby modify the surface-active sites of chitosan instead of forming ammonium cations.

The absence of the peak at 2354 cm^{-1} due to NH_3^+ for the 1 : 3 composite indicated the involvement of all the free $-NH_2$ groups of the chitosan for maximum electrostatic interactions with the IL molecules through the –OH groups of the sulfonic acid functionality. The peak at 2354 cm^{-1} also supported the existence of free ammonium cations within the structures of 1 : 1 and 1 : 2 chitosan–IL composites. Furthermore, the three composites (Fig. 3) retained all the characteristic assigned peaks of the 1 : 3 composites in Fig. 2 with comparable intensities except for slight shifting of the small peak around 500 cm^{-1} for the case of 1 : 3 composites.

The possible structure of the prepared adsorbent of chitosan with the sulfonic acid functionalized imidazolium [Mdsim]Cl ionic liquid could be represented in Fig. 4 involving intermolecular H-bonding interactions.

3.1.2. SEM analysis. The morphology of the 1 : 3 chitosan–IL composite was studied using SEM images as a representative sample as shown in Fig. 5. The chitosan–IL composite showed a reduction of agglomeration on its surface as compared to the non-uniform distribution of bigger aggregates for the chitosan sample. The surface roughness of chitosan was observed to decrease in the composite with the surface area increasing to 3.490 $m^2\ g^{-1}$ (from BET) compared to 2.99 $m^2\ g^{-1}$ for pure chitosan beads,[37] thereby enhancing the adsorption of MB dye. The MB dye adsorbed on the chitosan–[Mdsim]Cl composite represented a smooth surface morphology with uniform adsorption of the dye molecules by the chitosan–IL composite.

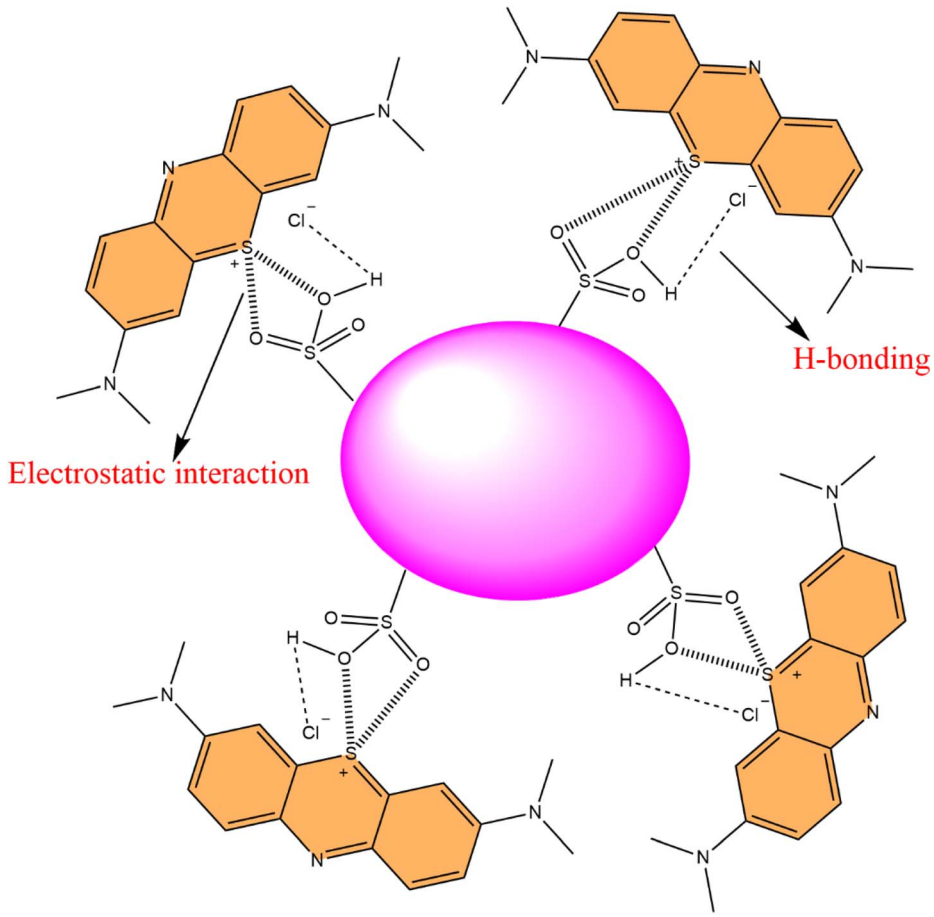

Scheme 3 Representative plausible interactions between the MB dye and the chitosan–IL composite.

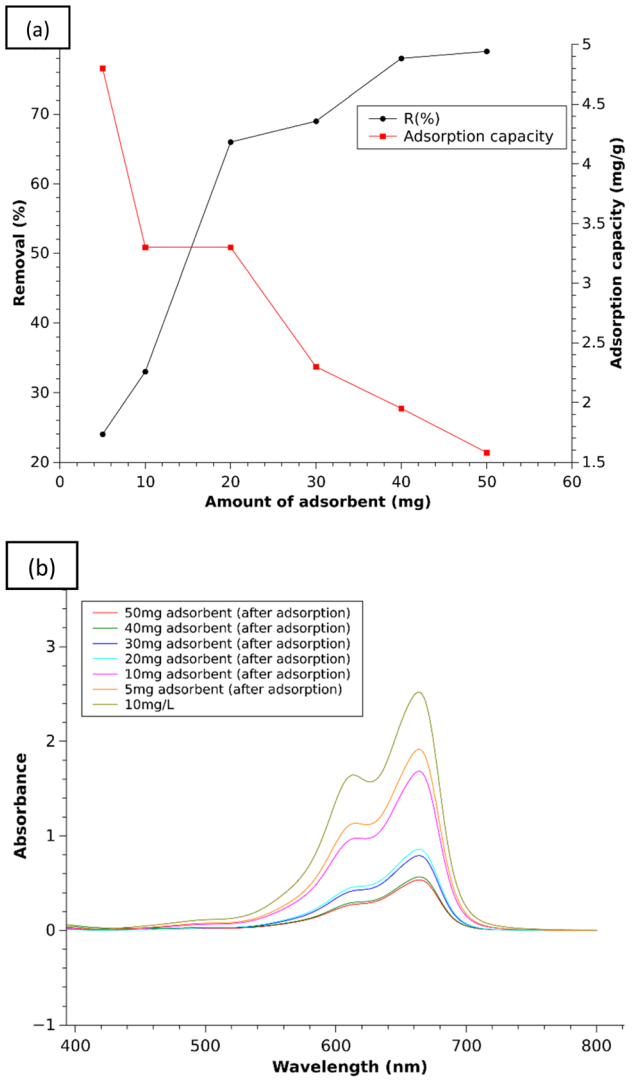

Fig. 10 (a) % Removal efficiency and adsorption capacity of the 1 : 3 composite with increasing amount and (b) UV plots of MB solution (10 mg L^{-1}) after adsorption with increasing amount of the 1 : 3 composite.

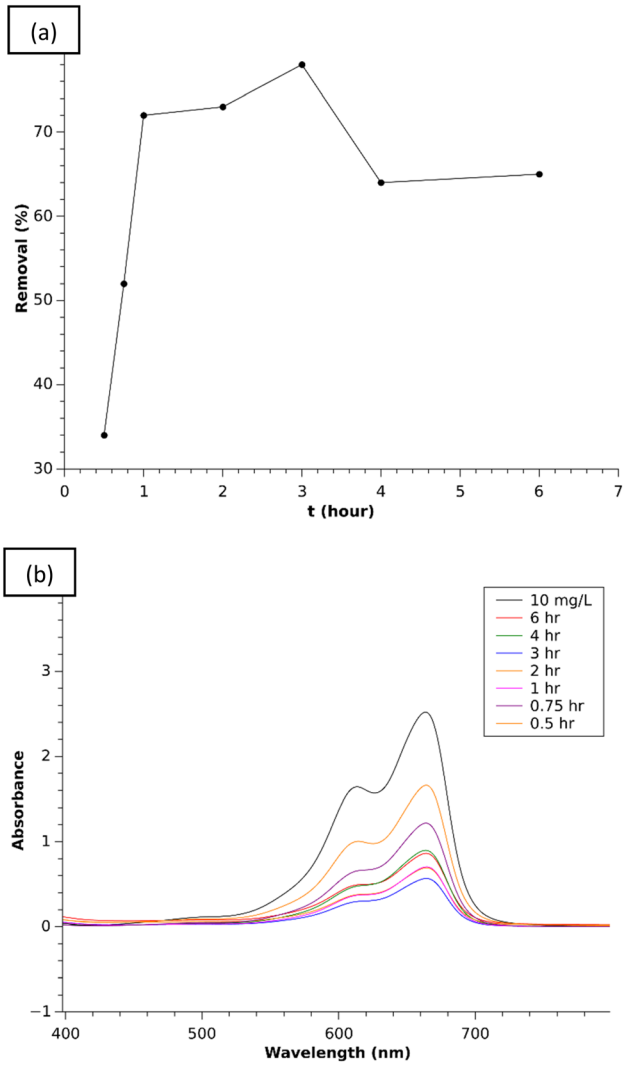

Fig. 11 (a) Effect of time on the adsorption behavior of the 1 : 3 composite and (b) UV plots for adsorption of MB solution (10 mg L^{-1}) during 6 h adsorption time using the 1 : 3 composite.

3.1.3. Powder X-ray diffraction study. The powder XRD pattern of the three chitosan–IL composites displayed one prominent peak at $2\theta = 19.80°$ in Fig. 6, which could be assigned to the characteristic peak of native chitosan at $2\theta = 20.1°$ (ref. 38) with slight shifting of the peak position to a lower 2θ value due to change of their crystalline structures by increasing *d*-spacing with respect to the bare chitosan. The surface modification of chitosan can also be confirmed by the existence of two medium sized broad humps around $2\theta = 30°$ and $2\theta = 40°$ for structural modification of the chitosan framework through involvement of interactions of various functional groups of chitosan including amino, hydroxyl and amide groups with the grafting sulfonic groups of imidazolium cations of the ionic liquid.[39]

3.1.4. Thermogravimetric analysis. The thermogravimetric analysis of the three composites of chitosan–IL in Fig. 7 showed identical thermal stabilities for the composites of 1 : 1, 1 : 2 and 1 : 3 ratios and chitosan up to 400 °C. Beyond this temperature, the 1 : 3 composite started stepwise decomposition with a retention of 5% mass residue above 500 °C. As compared to the 1 : 3 ratio, the degradation patterns of both the 1 : 1 and 1 : 2 ratios and chitosan were almost identical up to 600 °C. The three composites exhibited 10–15% gradual weight loss up to 250 °C, followed by another fast degradation of around 30% weight loss within 300 °C. Above 300 °C, for the lower IL loaded composites (1 : 1 and 1 : 2 ratios), a gradual loss of another 15% weight till 600 °C was observed instead of stepwise decomposition of the 1 : 3 composite. The higher degradation of the 1 : 3 composite at higher temperature may be attributed to the involvement of an excess amount of the loaded acidic IL for decomposition of the chitosan framework through interactions with various functional groups of chitosan.

3.1.5. BET analysis. Fig. 8 exhibited the nitrogen adsorption–desorption isotherm and the pore size distribution plot of

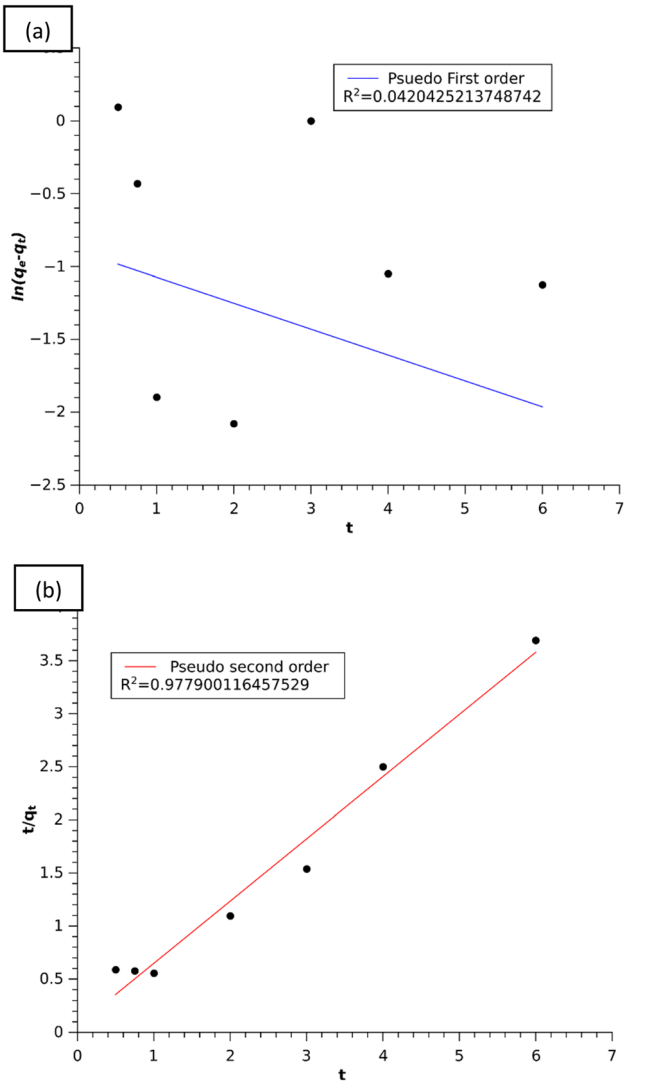

Fig. 12 (a) Linear plot of the pseudo-first order model and (b) linear plot of the pseudo-second order model.

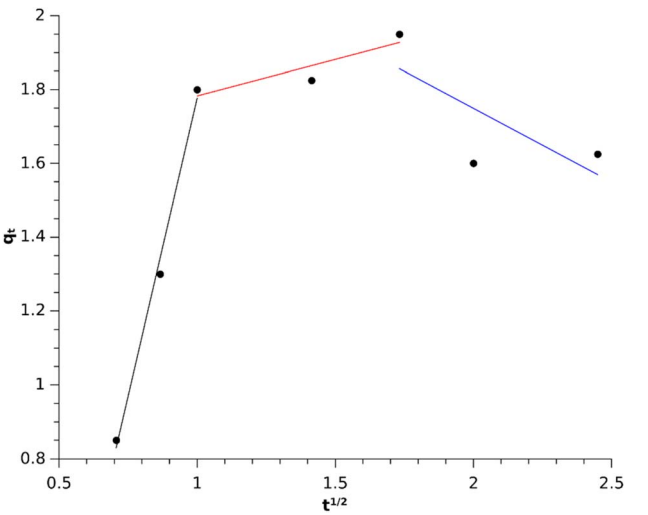

Fig. 13 Intra-particle diffusion model for MB adsorption.

the 1 : 3 composite using Quantachrome Instrument v11.05. The Brunauer–Emmett–Teller (BET) analysis showed a Type IV isotherm for the mesoporous structure with an H3 hysteresis lope, based on IUPAC classification.[40] Here capillary condensation was accompanied by hysteresis and resulted in a desorption curve higher than adsorption. The BET surface area was found to be 3.490 m^2 g^{-1}. From the BJH pore size distribution plot (Fig. 8(b)), the pore size and the total pore volume were determined to be 2.364 nm and 0.004 cm^3 g^{-1}, respectively.

3.2. Adsorption study

For screening of adsorption efficiency of the three composites with different loaded amounts of the ionic liquid as compared to chitosan, 40 mg of each of the sample was used for adsorption of the MB dye in 10 mL stock solution with 10 mg L^{-1} concentration by stirring the composite for 30 min at room temperature. The preliminary study showed rising adsorption efficiency of the 1 : 3 chitosan composite to 32% with respect to 8% adsorption efficiency in the case of chitosan as the bare adsorbent material (Fig. 9). These observations evidenced modifications of surface functionalities of the chitosan in the presence of the acidic imidazolium ionic liquid involving two –SO_3H groups attached to the imidazolium cation for the generation of a greater number of active sites for adsorption. A plausible interaction between the active sites of the adsorbent and the model dye molecule MB is proposed in Scheme 3.

Among the three composites, the 1 : 3 chitosan–IL composite was chosen for optimization of the amount of composite needed for maximum adsorption in 3 h for 10 mL of the MB stock solution (10 mg L^{-1}) with the gradual rise of the composite amount to 5, 10, 20, 30, 40 and 50 mg, respectively. The results are presented in Fig. 10(a) (Table S3†) by plotting the removal% of the dye against the amount of composite as the adsorbent material. The removal percentage of MB was found to be 28% for 5 mg of the composite, which increased to 78–79% corresponding to the amount of 40–50 mg of composite, respectively. This increasing trend of removal efficiency against the ascending order of the composite weights can be explained due to more available adsorption sites on the chitosan–IL composite after modification of chitosan surface functionalities for adsorption of the dyes. Beyond the amount of 40 mg, the increase of the removal percentage is found to be very low as the concentration of MB both on the surface and in solution may have reached equilibrium.[41] So, without further increasing the amount of composite, the optimum was fixed at 40 mg. Additionally, the removal efficiency for 20 and 30 mg L^{-1} of MB dye solutions was also studied with the optimized amount of composite (1 : 3) and found to be 47% and 19%, respectively.

With the optimized amount of 40 mg of composite, the effect of pH was studied to increase or decrease the removal percentages of MB at varied pH of the solution. The results showed the removal efficiencies of MB dye as 1% at pH 3, 80% at pH 10 and 79% at neutral pH. It was seen that the increased pH slightly increased the removal percentage of dye compared to the neutral solution. Therefore, the adsorption capacities of

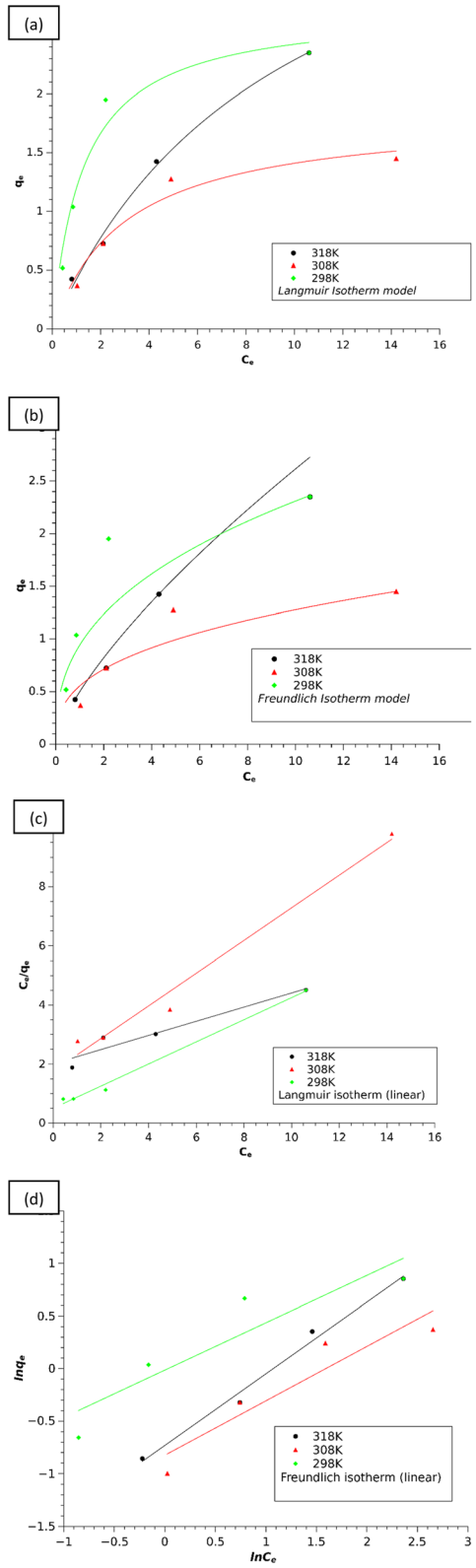

Fig. 14 The isotherms of dye adsorption on the 1 : 3 composite: (a) Langmuir isotherm, (b) Freundlich isotherm, (c) Langmuir isotherm (linear) and (d) Freundlich isotherm (linear).

Table 3 Calculated thermodynamic parameters for adsorption

Temperature (K)	ΔG^0 (J mol^{-1})	ΔH^0 (J mol^{-1})	ΔS^0 (J mol^{-1})
298	706.31	−72513.38	−245.475
308	2957.42		
318	5615.83		

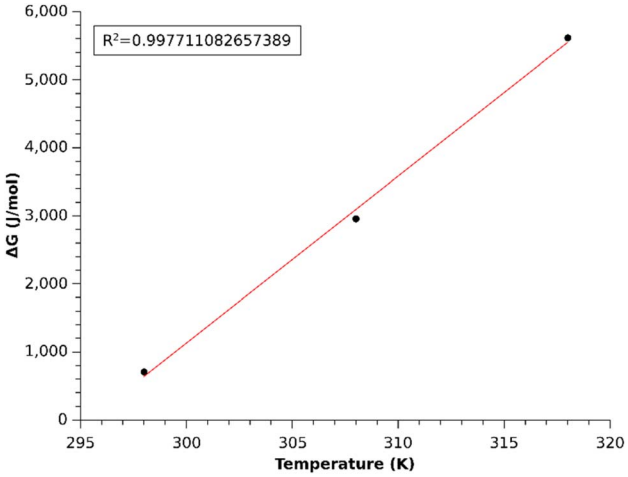

Fig. 15 Linear plot of ΔG *vs.* temperature.

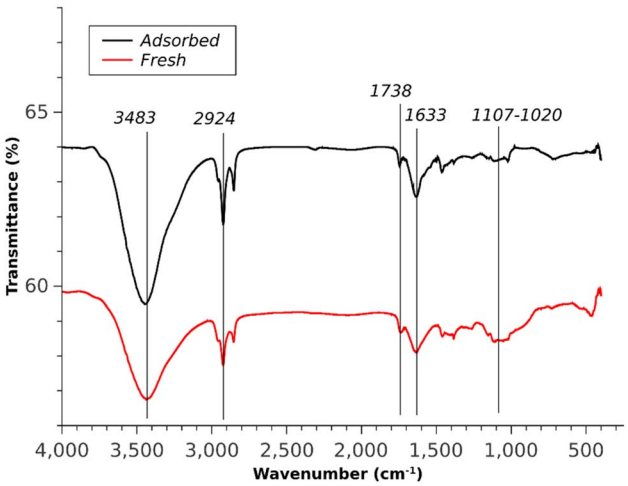

Fig. 16 FTIR spectra of fresh and adsorbed composites.

the 1 : 3 composite for different doses were calculated at neutral pH and are represented in Fig. 10(a).

This observation showed that by lowering the pH of solution, the surface of chitosan–IL generates protonated amino groups, leading to increasing repulsive interactions with the cationic MB dye and thereby lowering the removal efficiencies of MB dye. It could be expected that at pH 7–10, the surface of the chitosan–IL composite remains predominantly negatively charged due to SO_3^- groups, which adsorb cationic dye molecules.[42]

3.3. Adsorption kinetics study

The kinetic study of MB adsorption was carried out by stirring 40 mg of the composite (1 : 3 ratio) in 10 mL dye solution (10 mg L^{-1}) at different time intervals, *i.e.* $\frac{1}{2}$ h, 0.75 h, 1 h, 2 h, 3 h, 4 h and 6 h, in separate batches with simultaneous measurement of removal efficiency (%) of the dye. It was observed that after 3 h of adsorption, the composite enabled the maximum removal of the dye from the aqueous solution in Fig. 11. This figure showed that with increasing time from 30 min to 3 h, the removal efficiency rises from 34% to the maximum value of 78% respectively and again reduces to around 64% to 65% over a duration of 4–6 h. It can be expected that due to available adsorption sites in the composite material, the removal efficiency achieved the equilibrium position after 3 h from the start. Beyond that time, the adsorption equilibrium shifted to the reverse direction with a lowering of the removal efficiency value after 3 h.

The above experimental data were fitted with pseudo-first order (PFO) and pseudo-second order (PSO) kinetic eqn (4) and (5) as mentioned under the experimental section to find the adsorption kinetic parameters of MB adsorption on the composite (1 : 3 ratio) in Fig. 12.

The kinetic plot in Fig. 12(b) clearly showed that the adsorption of MB on the composite was well described by the pseudo-second order model with a higher regression coefficient of $R^2 = 0.9779$ than the pseudo-first order model and also the experimental value of $q_{e,exp}$ seems to be closer to the calculated $q_{e,cal}$ value of the pseudo-second order model as mentioned in Table 1. From these results, we can say that the pseudo-second-order kinetic model furnished the best interpretation of the MB adsorption mechanism. In this model, the rate limiting step is the surface adsorption that involves chemisorption in solution *via* physicochemical interactions between the adsorption sites of the adsorbent and the concentration of the adsorbate.[43] Furthermore, this model assumes that the rate of adsorption on active sites is proportional to the square of unoccupied sites of the absorbent and the number of occupied sites proportional to the fraction of the adsorbate attached to the adsorbent surface.[3]

The experimental data were also used to understand the intraparticle diffusion model of Weber–Morris using eqn (6). The plot in Fig. 13 showed three stages of adsorption onto the composite, *i.e.* bulk, film and intra-particle diffusion. The 1st stage could be attributed to instantaneous adsorption of MB on the exterior active sites of the adsorbent till all the sites were occupied. This was followed by slow diffusion of the MB molecules into the pores of the adsorbent as observed in the second and third linear portions of the graph, which evidenced the existence of the intra-particle diffusion mechanism in the adsorption process.[34] The higher value of K_{i1} than K_{i2} and K_{i3} (Table 1) showed that the adsorption of MB onto the composite is controlled by the bulk diffusion stage.

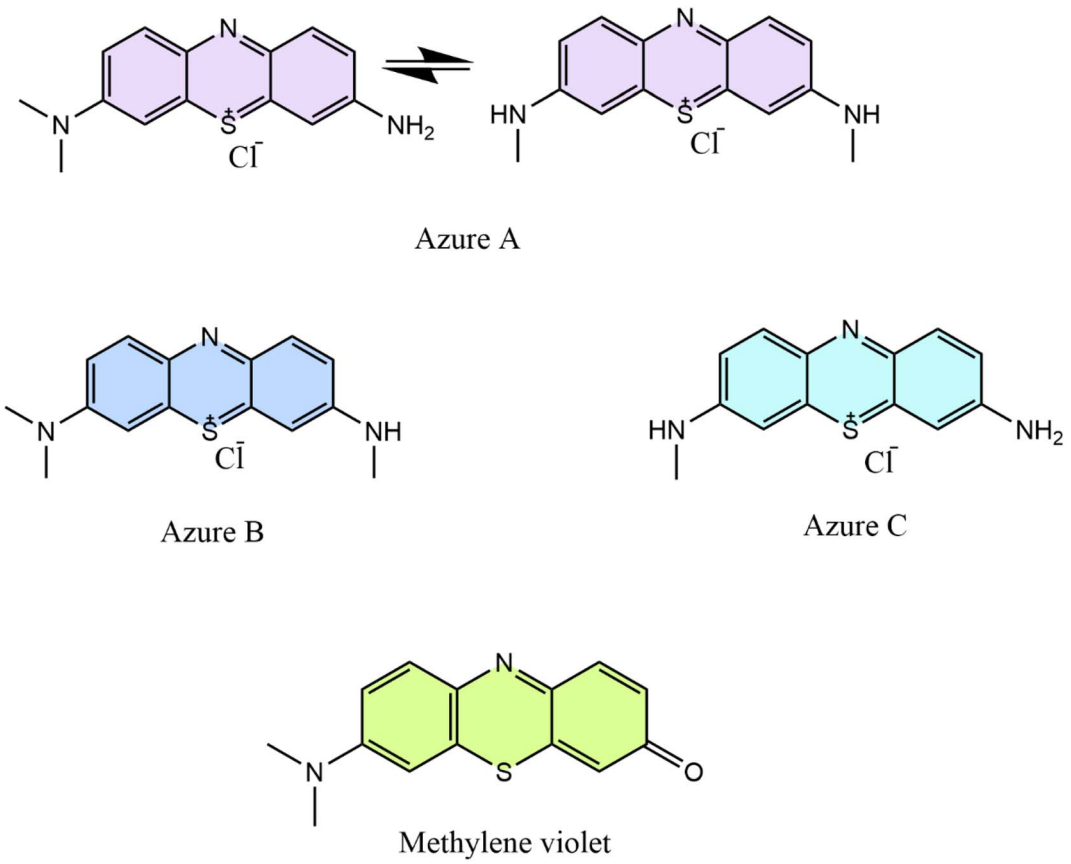

Fig. 17 Structures of oxidative degradation products of MB by an alkali.

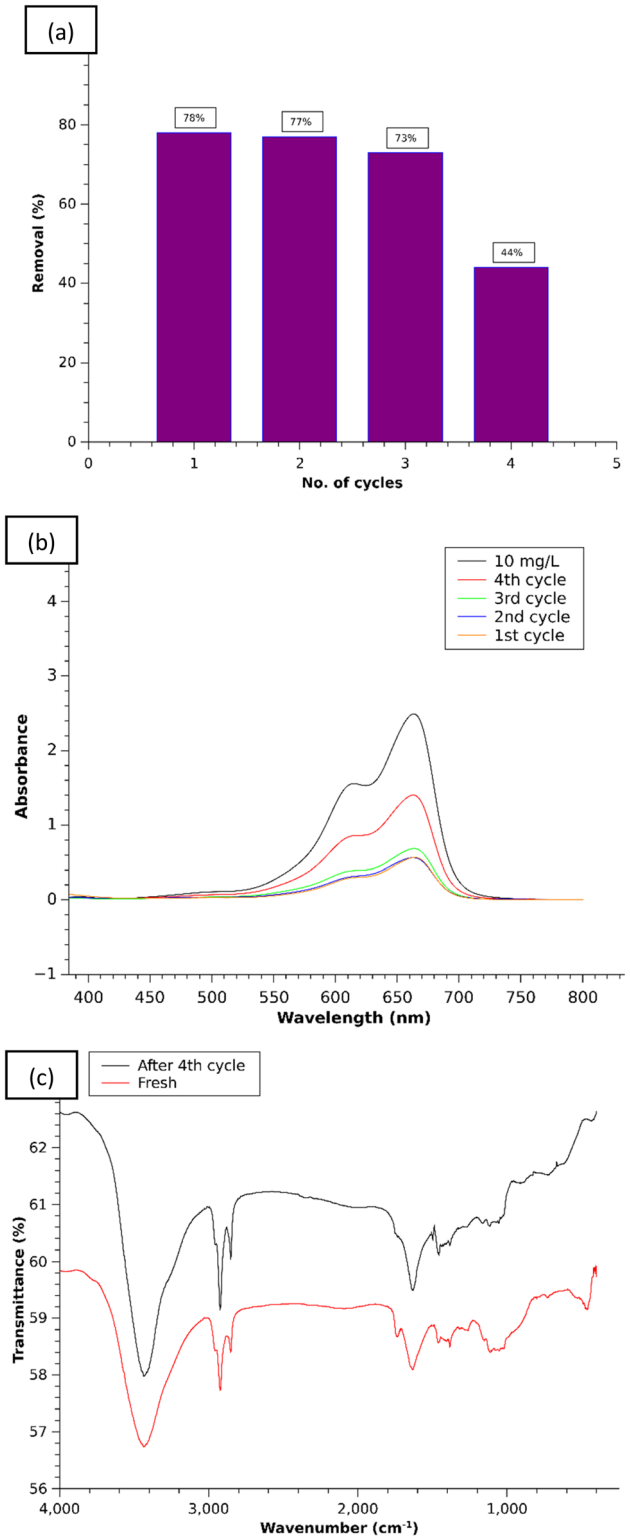

Fig. 18 (a) Bar diagram of the removal% of MB for the reused 1 : 3 composite, (b) UV-Vis study for the recycled composite and (c) comparative FT-IR spectra of 1 : 3 reused and fresh composites.

3.4. Adsorption isotherm study

To study the adsorption isotherm of the composite material, 40 mg of the composite (1 : 3 ratio) was employed to adsorb MB dye solutions of varied concentrations (2.5, 5, 10 and 20 mg L^{-1}) in 3 h for determination of the adsorption capacity (q_e) of the composite and the equilibrium concentration of the dye (C_e) at each temperature (*i.e.* 298, 308, and 318 K) (Table S2†). The well-known adsorption isotherm eqn (6) for the Langmuir model and eqn (7) for the Freundlich model as given in sub-unit 2.6 of experimental section were used to evaluate the experimental data of adsorption of MB dyes (Table S2†) with variation of the MB concentrations and temperature of the adsorption experiment.[28] The isotherms of dye adsorptions are included in Fig. 14.

The isotherm model parameter values (Table 2) obtained from the isotherms (Fig. 14) showed that the adsorption of MB on the composites well fits the Langmuir isotherm model, which suggests that the adsorption occurs on the homogeneous sites through monolayer coverage.[28]

The suitability of the adsorption process can be determined from the separation factor R_L using the expression in eqn (11),[28]

$$R_L = \frac{1}{1 + K_L C_0} \tag{11}$$

where K_L is the Langmuir constant. The value of $0 < R_L < 1$ suggests a favorable adsorption process and the calculated value of R_L from Table 2 shows that the adsorption of MB on the composites is favorable.

3.5. Thermodynamic studies

To find the feasibility, spontaneity, and nature of adsorption, the values of thermodynamic parameters, *i.e.*, change in Gibbs free energy, change in enthalpy, and change in entropy, were determined using the Van't Hoff eqn (12) and (13),[28]

$$\Delta G^0 = -RT \ln K_L \tag{12}$$

$$\Delta G^0 = \Delta H^0 - T\Delta S^0 \tag{13}$$

where T is the temperature (K), R is the gas constant (8.314 J mol^{-1} K^{-1}) and K_L is the Langmuir constant. The calculated values in Table 3 obtained from the linear plot in Fig. 15 showed that the G^0 value increases with an increase in temperature, indicating that the adsorption is favorable at lower temperature. Also, the negative H^0 value indicated that the adsorption process is exothermic in nature.

3.6. Mechanism of adsorption study

A plausible interaction between the active sites of the adsorbent and the model dye molecule MB is displayed in Scheme 3, where the electrostatic interactions observed between the functionalized –SO_3H surfaces of the chitosan–IL adsorbent with the partial positive sites of heteroatoms of cationic dyes. Other possible binding interactions included H–bonding acceptor sites of the dye such as Cl^- counter ions with the acidic proton of sulfonic acid tethered on the surface of the chitosan–IL adsorbent.

The existence of strong intermolecular H-bonding interactions in the MB adsorbed composite was evidenced from the comparative FT-IR spectrum of the MB adsorbed chitosan–IL

(1 : 3) composite with the fresh 1 : 3 composite (Fig. 16). The dye adsorbed composite exhibited suppression of the wide peak position of the fresh composite centered at 1100 cm^{-1} in addition to sharpening of peak intensities of the O–H and N–H merged stretching bands. The increasing intensity of the O–H peak can be considered as an outcome of partial reduction of intermolecular H-bonding after the adsorption of the MB dye on its surfaces.

3.7. Desorption and recyclability

For regeneration of the composite, the used 1 : 3 chitosan–[Mdsim]Cl composite from the first cycle was kept in 10 mL of 2 M NaOH solution (pH = 14) for 24 hours to leach out the adsorbed dye from the composite. As the concentration of NaOH increases, the negatively charged surface of the chitosan–IL adsorbent[42,44] would prefer to interact with the smaller sized Na^+ cation due to its high charge density as compared to partial positive charge containing bulkier cationic dye. This may lead to weakening of electrostatic interactions of adsorbed cationic MB dye through the active sites of the sulfonic acid group of the chitosan–IL composite and then initiate the desorption of dye molecules to the alkaline solution. Later, the desorbed MB dye would undergo oxidative degradation gradually to intermediate dyes Azure B, Azure A, Azure C and Bernthsen methylene violet (MVP) (Fig. 17) as per a reported mechanism[45–48] *via* successive *N*-demethylation and deamination reactions. Subsequently, further decomposition of the intermediate dyes of MB degradation in alkaline solution may produce low molecular weight homologous MB derivatives at a longer reaction time.[48,49] As already observed, the desorption of MB from the surface of the chitosan–IL composite did not occur up to pH 10 for which a lower concentration of the alkaline solution was not employed.

The regenerated composite was separated from the dye solution through filtration and washed with excess water. It was again reused for the second cycle after drying in the air for 24 h and these steps were repeated up to 4 cycles. Fig. 18 shows that the efficiency of the composite almost remained the same up to 3 cycles and then onwards the removal percentage decreased to 44%. The FTIR spectrum (Fig. 18) of the used composite displayed a slight change of the peak position in the fingerprint region of FTIR as compared to the fresh composite after the 4th cycle. The lowering of the removal percentage of the composite could be attributed to the repeated washing with alkaline solution, which may cause leaching of the immobilized [Mdsim]Cl ionic liquid into water media.

Table 4 Comparison of different dyes

Dye	Adsorption time (hours)	Adsorption capacity (mg g^{-1})
Methylene blue	3	1.94
Crystal violet	18	1.825
Methyl green	3	2.1
Methyl orange	18	0.975

3.8. Adsorption of different dyes

The adsorption capacity of the composite was also compared for other dyes like crystal violet, methyl green and methyl orange and the results are illustrated in Table 4 obtained from Fig. 19.

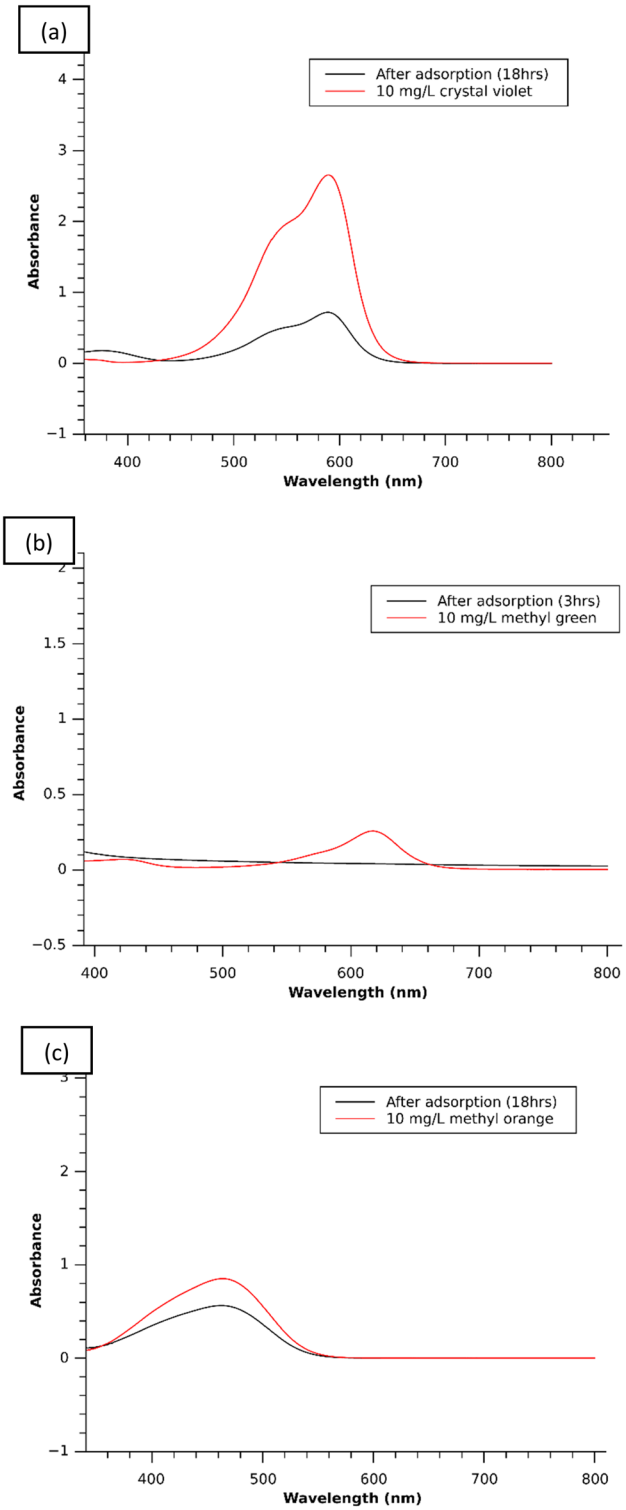

Fig. 19 UV study adsorption plots of the 1 : 3 composite using different dyes: (a) crystal violet, (b) methyl green and (c) methyl orange.

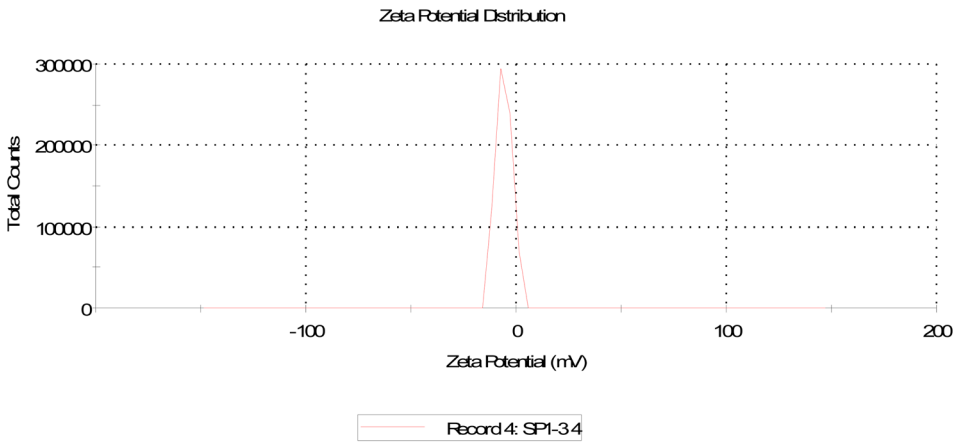

Fig. 20 Zeta potential study of the composite (1 : 3).

This was done by employing 40 mg of the 1 : 3 composite in 10 mL of the aqueous dye solutions (10 mg L^{-1}) at room temperature for a certain period. It was seen that the methyl orange showed the lowest adsorption capacity among the four dye molecules. The differences in the adsorption capacities (Table 4) of the studied dyes by the negatively charged surfaces of chitosan–IL composites could be correlated to the nature of binding sites of cationic or anionic dyes. The results in Table 4 indicated strong electrostatic binding interactions between the cationic dyes (MB, MG and CV) and the modified sulfonic acid functionalized surfaces of chitosan–IL adsorbents as compared to the anionic dye MO.

3.9. Zeta potential analysis

The zeta potential of the composite (1 : 3) was determined using a Zetasizer (Nano ZS90 Malvern Analytical) with a He–Ne laser equipped with a built-in temperature controller. The dispersant medium was water at neutral pH for the solid composites and the temperature was set at 25 °C. The zeta potential of the composite was found to be negative, as shown in Fig. 20. It can be said that the surface of the composite is negatively charged, which helps in absorbing the cationic dye MB on the surface by electrostatic interaction.[50]

4. Conclusions

This study described the fabrication and characterization of sulfonic acid functionalized imidazolium ionic liquid [Mdsim]Cl impregnated chitosan composites in three different w/w ratios of chitosan and ionic liquid (1 : 1, 1 : 2 and 1 : 3) by the wet impregnation method. Among the three composites, the 1 : 3 composite exhibited the maximum adsorption capacity of aqueous MB (10 mg L^{-1}) solution in 3 hours using the same amount of the composites at room temperature. The results revealed that MB adsorption was significantly increased by the composites with increasing amount of the acidic ionic liquid. The adsorption kinetics of MB was well described by a pseudo-second-order model and intra-particle diffusion model. It also followed the Langmuir adsorption isotherm and showed the maximum adsorption capacity of the MB dye using the 1 : 3 composite among the four studied dye compounds. The thermodynamic analysis showed the exothermic nature of the adsorption process by giving positive H^0 values. The recyclability of the composite was successfully demonstrated up to the 3rd cycles, with nearly the same removal efficiencies retained in the spent composites.

Data availability

The data that support the findings of this study are available in the ESI† of this article.

Author contributions

Subham Paul: methodology; data curation; investigation; formal analysis; writing – original draft. Amlan Jyoti Gogoi: investigation; formal analysis. Krishna Dev: validation; Prapti Priyam Handique: investigation. Debanga Bhusan Bora: validation; visualization. Sangeeta Kalita: formal analysis. Ruli Borah: conceptualization; methodology; supervision; writing – review & editing.

Conflicts of interest

There are no conflicts to declare.

Acknowledgements

The authors acknowledge the support of the Sophisticated Analytical Instrumentation Centre, Tezpur University for the analysis of various samples.

References

1 Y. Wang, H. Wang, H. Peng, Z. Wang, J. Wu and Z. Liu, *Fibers Polym.*, 2018, **19**, 340–349.
2 V. S. Munagapati, V. Yarramuthi and D. S. Kim, *J. Mol. Liq.*, 2017, **240**, 329–339.

3 B. Doshi, A. Ayati, B. Tanhaei, E. Repo and M. Sillanpää, *Carbohydr. Polym.*, 2018, **197**, 586–597.
4 M. Khadhraoui, H. Trabelsi, M. Ksibi, S. Bouguerra and B. Elleuch, *J. Hazard. Mater.*, 2009, **161**(2–3), 974–981.
5 M. F. Elahmadi, N. Bensalah and A. Gadri, *J. Hazard. Mater.*, 2009, **168**(2–3), 1163–1169.
6 M. D. Murcia, M. Gómez, E. Gómez, J. L. Gómez and N. Christofi, *Desalination*, 2011, **281**, 364–371.
7 L. Pereira, P. Dias, O. S. G. P. Soares, P. S. F. Ramalho, M. F. R. Pereira and M. M. Alves, *Appl. Catal. B Environ.*, 2017, **212**, 175–184.
8 M. Herrero and D. C. Stuckey, *Chemosphere*, 2015, **140**, 119–128.
9 K. Li, P. Li, J. Cai, S. Xiao, H. Yang and A. Li, *Chemosphere*, 2016, **154**, 310–318.
10 M. Chafi, B. Gourich, A. H. Essadki, C. Vial and A. Fabregat, *Desalination*, 2011, **281**, 285–292.
11 G. Ciardelli, L. Corsi and M. Marcucci, *Resour., Conserv. Recycl.*, 2001, **31**(2), 189–197.
12 T. A. Aragaw and F. M. Bogale, *Front. Environ. Sci.*, 2021, **9**, 764958.
13 I. Suyambulingam, L. Gangadhar, S. S. Sana, D. Divakaran, S. Siengchin, L. A. Kurup and K. E. Albert Bernad Noble, *Adv. Mater. Sci. Eng.*, 2023, **1**, 9387016.
14 Y. Yang, Y. Li, K. Goh, C. H. Tan and R. Wang, *J. Membr. Sci.*, 2021, **620**, 118833.
15 D. Gomez-Maldonado, I. B. Vega Erramuspe and M. S. Peresin, *BioResources*, 2019, **14**(4), 10093–11016.
16 D. R. Johnson, M. M. Methner, A. J. Kennedy and J. A. Steevens, *Environ. Health Perspect.*, 2010, **118**(1), 49–54.
17 F. Naseeruteen, N. S. A. Hamid, F. B. M. Suah, W. S. W. Ngah and F. S. Mehamod, *Int. J. Biol. Macromol.*, 2018, **107**, 1270–1277.
18 G. Crini and P. M. Badot, *Prog. Polym. Sci.*, 2008, **33**(4), 399–447.
19 M. H. Dehghani, A. Dehghan, H. Alidadi, M. Dolatabadi, M. Mehrabpour and A. Converti, *Korean J. Chem. Eng.*, 2017, **34**, 1699–1707.
20 Y. L. Pang, J. H. Tan, S. Lim and W. C. Chong, *Polymers*, 2021, **13**(17), 3009.
21 W. W. Ngah, L. C. Teong and M. M. Hanafiah, *Carbohydr. Polym.*, 2011, **83**(4), 1446–1456.
22 A. Ayati, S. Ranjbari, B. Tanhaei and M. Sillanpää, *J. Mol. Liq.*, 2019, **275**, 71–83.
23 S. K. Singh and A. W. Savoy, *J. Mol. Liq.*, 2020, **297**, 112038.
24 Z. Lei, B. Chen, Y. M. Koo and D. R. MacFarlane, *Chem. Rev.*, 2017, **117**(10), 6633–6635.
25 N. Nasirpour, M. Mohammadpourfard and S. Z. Heris, *Chem. Eng. Res. Des.*, 2017, **160**, 264–300.
26 N. F. Alqahtani, *React. Funct. Polym.*, 2023, 105779.
27 A. K. Dutta, P. Gogoi and R. Borah, *RSC Adv.*, 2014, **4**(78), 41287–41291.
28 S. Ranjbari, B. Tanhaei, A. Ayati, S. Khadempir and M. Sillanpää, *Int. J. Biol. Macromol.*, 2020, **155**, 421–429.
29 Y. Huang, S. Li, J. Chen, X. Zhang and Y. Chen, *Appl. Surf. Sci.*, 2014, **293**, 160–168.
30 M. N. Sepehr, V. Sivasankar, M. Zarrabi and M. S. Kumar, *Chem. Eng. J.*, 2013, **228**, 192–204.
31 Y. S. Ho, *J. Hazard. Mater.*, 2006, **136**(3), 681–689.
32 W. J. Weber Jr and J. C. Morris, *J. Sanit. Eng. Div.*, 1963, **89**(2), 31–59.
33 S. Hosseini, M. A. Khan, M. R. Malekbala, W. Cheah and T. S. Choong, *Chem. Eng. J.*, 2011, **171**(3), 1124–1131.
34 B. Tanhaei, A. Ayati, M. Lahtinen and M. Sillanpää, *Chem. Eng. J.*, 2015, **259**, 1–10.
35 S. Das, T. Dutta and R. Borah, *J. Mol. Liq.*, 2019, **289**, 111099.
36 I. A. Oxton, O. Knop and M. Falk, *Can. J. Chem.*, 1975, **53**, 2675–2682.
37 S. Hasan, T. K. Ghosh, D. S. Viswanath and V. M. Boddu, *J. Hazardous Materi*, 2008, **152**, 826–837.
38 A. S. K. Kumar, C. U. Kumar, V. Rajesh and N. Rajesh, *Int. J. Biol. Macromol.*, 2014, **66**, 135–143.
39 A. S. K. Kumar, C. U. Kumar, V. Rajesh and N. Rajesh, *Int. J. Biol. Macromol.*, 2014, **66**, 135–143.
40 M. Thommes, K. Kaneko, A. V. Neimark, J. P. Olivier, F. Rodriguez-Reinoso, J. Rouquerol and K. S. Sing, *Pure Appl. Chem.*, 2015, **87**(9-10), 1051–1069.
41 T. K. Naiya, A. K. Bhattacharya and S. K. Das, *J. Colloid Interface Sci.*, 2009, **333**(1), 14–26.
42 C. Li, Y. He, L. Zhou, T. Xu, J. Hu, C. Peng and H. Liua, *RSC Adv.*, 2018, **8**, 41986–41993.
43 H. Wang, A. Zhou, F. Peng, H. Yu and J. Yang, *J. Colloid Interface Sci.*, 2007, **316**(2), 277–283.
44 M. Vakili, S. Deng, L. Shen, D. Shan, D. Liu and G. Yu, *Sep. Purif. Rev.*, 2017, 1–13.
45 A. Katafias, M. Lipinska and K. Strutynski, *Reac Kinet. Mech. Cat*, 2010, **101**, 251–266.
46 M. Havelcova, P. Kuba and A. NeÏmcova, *Dyes Pigm.*, 2000, **44**, 49–54.
47 A. Mills, D. Hazafy, J. Parkinson, T. Tuttle and M. G. Hutchings, *Dyes Pigm.*, 2011, **88**, 149e155.
48 W. C. Holmes and B. W. French, *Stain Technol.*, 1926, **1**, 17–26.
49 A. Zubrik, D. Jáger, E. Mačingová, M. Matik and S. Hredzák, *Sci. Rep.*, 2023, **13**, 14773.
50 M. Lai, P. Liu, H. Lin, Y. Luo, H. Li, X. Wang and R. Sun, *Carbohydr. Polym.*, 2016, **137**, 375–381.